Stark Effect of Intrinsic and Extrinsic Charge-Transfer Excitons in a Linear Donor−Acceptor Stack: Anthracene−Pyromellitic Dianhydride

Gerhard Weiser* and Andreas Elschner

Fachbereich Physik, Philipps-Universität Marburg, 35032 Marburg, Germany, and H.C. Starck GmbH, Chemiepark Leverkusen, Germany

Received: February 12, 2009; Revised Manuscript Received: May 6, 2009

Anthracene−PMDA single crystals display at 2K about 70 meV below a well-known intrinsic charge-transfer exciton three narrow absorption lines, which are attributed to CT excitons bound to defects of a few 10^{-5} concentration. All excitons respond very sensitively to electric fields along the molecular stack because of the large dipole moment, about 2 eÅ, of an ionized donor−acceptor pair, but only intrinsic excitons observe an optical selection rule. Although the triclinic unit cell contains only one pair of molecules, excitons appear in field-modulated spectra as near-degenerate doublets of different parity with very small splitting. The line shape of the EA spectra and selection rules with respect to the polarization of light and orientation of the field are consistent with the inversion symmetry of the lattice and the molecules. The simple crystal structure enables identification of the defects that are responsible for extrinsic excitons. Symmetry consideration based on translation invariance lead to a new interpretation of intrinsic excitons as true crystal states with charge transfer from the donor to the acceptor sublattice.

1. Introduction

Weak charge-transfer compounds consist of two types of molecules with a nearly neutral ground state. Optical excitation leads to charge transfer resulting in partially ionized molecules and an absorption band below the gaps of intramolecular transitions. Because intermolecular transitions require spatial overlap of molecular orbitals, charge-transfer crystals represent a class of solids that is intermediate between molecular crystals with weakly interacting molecules and solids with a network of covalent bonds. Intramolecular transitions split in molecular crystals by dipolar coupling according to the symmetry of the unit cell,[1] and intersite hopping broadens atomic and molecular states to energy bands. Optical transitions between strongly hybridized atomic states of wide band semiconductors still reflect the symmetry of atomic states, but translation invariance of electron states in a periodic potential imposes additional selection rules.[2] Such long-range coupling is often neglected in organic solids where spectra are dominated by molecular singlet excitons. A local approach also seems to be sufficient for describing the intermolecular transition of charge-transfer compounds, which changes a neutral to an ionic pair of donor and acceptor molecules.[3] The transformation into an ionic pair couples the exciton to molecular vibrations and lattice modes, and the corresponding spectral broadening prevents a detailed analysis of the electronic structure. A rare exception is the 1:1 compound An−PMDA (anthracene−pyromellitic dianhydride), which became representative of weak charge-transfer crystals with mixed stacks of molecules. They differ by their neutral ground state from strong charge-transfer compounds with ionic ground state and molecules arranged in segregated stacks that often show metallic properties.[4]

Because charge transfer generates a large dipole moment, the excited state should be sensitive to an electric field, but early attempts to measure field-modulated spectra were disappointing. The response of an intramolecular charge transfer in dichloroanthracene was very weak.[5] Studies on thin films of anthracene resolved the CT excitons, although they were hidden under the strong progression of the intramolecular exciton,[6] and the analysis of two CT absorption bands in polyvinylcarbazole−trintrofluorenone was hampered by large inhomogeneous broadening.[7] Single crystals of many CT compounds display at low temperatures well-resolved vibronic bands, but field-modulated spectra were not reported. The situation changed with the discovery of a purely electronic transition in luminescence[8] and absorption spectra[9,10] in single crystals of An−PMDA grown from highly purified material. Reflectance spectra at low temperature[11] led to an elaborate model of excitons based on donor−acceptor pairs with vibronic and phonon coupling, which is summarized in a review article.[12] The large dipole moment of the CT exciton was determined from the shift of the absorption peak in a static electric field[13,14] and confirmed by electroreflectance spectra, which resolved the excitonic zero-phonon line (ZPL) on the leading edge of several vibronic bands.[15] The sensitivity of the CT exciton to an electric field results only partially from the large charge-transfer dipole, μ_{CT}; the inversion symmetry of the crystal that is broken by the electric field is just as important. Piezo-modulated spectra using symmetry-conserving strain indeed did not show a particular sensitivity of the charge-transfer exciton.[16] Crystal quality and narrow line width facilitate such studies, and samples of An−PMDA that do not resolve the ZPL in reflectance show electroreflectance spectra with strongly reduced amplitude.[17] Transient absorption spectroscopy confirmed the CT exciton as coherent eigenstate[18] but did not support the interesting idea of exciton strings conjectured from earlier pump−probe experiments.[19]

The intermolecular charge transfer explains the orientation of the charge CT dipole along the molecular stack but not the optical selection rule of the transition between two large molecules in a low symmetry lattice. We present here a supplementary study of field-modulated spectra of extrinsic excitons, which differ from intrinsic excitons by the absence

* Corresponding author. E-mail: weiser@staff.uni-marburg.de.

10.1021/jp901300k CCC: $40.75 © 2009 American Chemical Society
Published on Web 05/29/2009

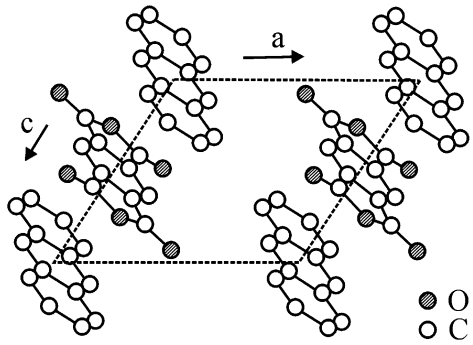

Figure 1. View on the *ac* plane showing the mixed molecular stacks along the *c* axis.

TABLE 1: Crystal Parameter of An−PMDA at −120 °C[22]

a (Å)	*b* (Å)	*c* (Å)	α	*β*	*γ*
7.2812	10.7684	7.1246	117.51	111.513	97.437

volume = 429.65 Å^3, $Z = 1$, $M = 396.36$ g·mol^{-1}

of an optical selection rule and different coupling to low frequency modes. Because no calculations of wave functions and matrix elements of sufficient accuracy exist, the analysis of extrinsic and intrinsic excitons rests on the symmetry of the crystal and the molecules and on principles of perturbation theory. This approach reveals a fundamental inconsistency of the current model for the Stark effect of intrinsic excitons that disappears if translation invariance of crystal states is included.

2. Crystal Structure and Experimental Details

High-quality crystals were grown from zone-refined material by vacuum sublimation[20] at temperatures in the range between 190 and 210 °C close to the melting point 513 K of the stable equimolar mixture of anthracene and PMDA.[21] Figure 1 presents a view on the (010) plane. The triclinic unit cell contains a single pair of molecules and imposes no symmetry-based selection rule. The crystal space group is $P\bar{1}$ because the stacking of centrosymmetric molecules along the *c* axis with distance *c*/2 introduces inversion symmetry with each molecular site being an inversion center. The molecular planes are tilted by 21° against *c*, which seems to be favorable for enhanced spatial overlap of the HOMO state of the donor anthracene and the LUMO of the acceptor PMDA.[12] The lattice constants in Table 1[22] reveal the large separation of identical molecules and point to the negligible hybridization of molecular states, except along the stacking axis *c*. The compound thus consists of two identical Bravais sublattices with a single molecule on the lattice sites, which under illumination exchange charge, which makes that CT exciton a true eigenstate of the compound crystal. The large separation of molecular stacks suggests a 1D character of the crystal states, which is supported by a large anisotropy of drift mobilities.[23] By far, the highest mobility is found for electrons moving along the *c* axis, which indicates stronger coupling of the molecular LUMO states than of their HOMO states. Pronounced anisotropy of molecular coupling is also apparent in the much faster thermal expansion of the *c* axis at room temperature.[24]

All spectra were taken under normal incidence of light from the (010) face with lateral size of 4 to 5 mm. Evaporated Ag contacts supplied a sinusoidal voltage of 1 kHz frequency across a 0.5 mm wide gap. The field-induced change, ΔI, of the transmitted light intensity occurs at twice that frequency and was measured by conventional lock-in technique simultaneously recording the intensity of light. The samples were immersed in superfluid He to reduce thermal broadening because modulated spectra taken at 10 K were already reduced by two orders of magnitude. Light of a tungsten halide lamp was dispersed by a 1 m monochromator polarized by a calcite polarizer and focused into the gap between the electrodes. Light intensities were measured by a photomultiplier, and the transmittance is obtained as A ratio of intensities with and without the sample in the optical path. We accounted for loss by reflectance by setting the absorption constant at low energy to zero, which has no effect on the evaluation of the absorption constant and the electroabsorption signal. Narrow slits (50 μm) set the spectral bandpass to 0.15 meV for transmission measurements, and about twice the bandpass is used in electroabsorption studies to improve the signal-to-noise ratio.

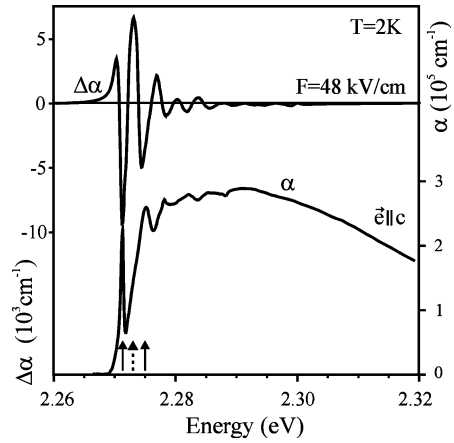

Figure 2. Absorption (bottom) and electroabsorption spectra with field $F\|c$ in the region of the 0−0 intrinsic charge-transfer band.

The large electrode spacing provided a homogeneous field for electroreflectance studies of the intrinsic CT exciton because of the small penetration depth of light but not for electroabsorption because of a large thickness of the samples up to 2 mm. Larger electrode spacing could not be used because sparking across the contact limited the peak voltage to 2.5 kV, and cleaving deteriorated the quality of the samples. Because field-induced changes of the reflectance are negligible in the transparent region, the electroabsorption spectrum, $\Delta\alpha$, is given by the ratio of the relative change of the transmitted intensity and the sample thickness, *d*.

$$\Delta\alpha = -\frac{1}{d}\frac{\Delta I}{I} \tag{1}$$

3. Experimental Results

3.1. Intrinsic Charge-Transfer Exciton. This section reviews the properties of the intrinsic CT exciton and the current model of its Stark effect. Figure 2 displays absorption and electroabsorption spectra in the range of the 0−0 absorption band derived by Kramers−Kronig transformation of published electroreflectance data.[15] The absorption shows the ZPL of the charge-transfer exciton and a phonon progression of 3.6 meV energy.[11] Full arrows mark the position of the ZPL at 2.2715 eV of the dipole-allowed exciton, Φ_u, and its first satellite, whereas the dashed arrow shows the position of a dark exciton state, Φ_g. Charge transfer in a unit cell creates an ionic pair A^-D^+, but the resulting permanent dipole, μ_p, is not compatible with the inversion symmetry of the crystal. Excitons, $\Phi_{g,u}$, of even and odd parity, $\Phi_{g,u}$, that satisfy inversion symmetry have been modeled by symmetric and antisymmetric combination of

dipoles of opposite sign in trimer configurations, DA^-D^+ and D^+A^-D, which interact by intersite hopping of the hole or of the electron in configurations such as A^-D^+A.[14,15]

$$\Phi_{g,u} = \frac{1}{\sqrt{2}}(A^-D^+ \pm D^+A^-) \tag{2}$$

The transition energies are derived by diagonalization of the corresponding Hamiltonian of the excited donor−acceptor pair of energy, E_{CT}, and an off-diagonal element V accounts for their splitting.[25]

$$E_{u,g}(F) = \begin{bmatrix} A^-D^+ & V \\ V & D^+A^- \end{bmatrix} = E_{CT} \pm V \tag{3}$$

The splitting of the dipole-allowed and -forbidden state, 2 V ≃ 1.6 meV, is surprisingly small for an intersite hopping matrix element, which enables moderate electric fields, F, to overcome that splitting. Excitons are converted back to ionized pairs, $\Phi_{1,2}$, with charge-transfer dipoles, μ_{CT}, of opposite sign, which split apart by a linear Stark effect.

$$E_{1,2}(F) = \begin{bmatrix} E_u & \mu_{CT}F \\ \mu_{CT}F & E_g \end{bmatrix} = E_{CT} \pm \sqrt{V^2 + (\mu_{CT}F)^2} \tag{4}$$

Evaluation of the Stark shift yields a dipole moment μ_{CT} = 2.3 eÅ, which shows that 2/3 of an electron charge is transferred in the optical transition over the donor−acceptor distance. At 40 kV/cm, $\mu_{CT}F$ exceeds V, and a pair of narrow exciton peaks of equal strength appears in reflectance spectra,[15] whereas the absorption spectrum resolves a second ZPL that rises with increasing field.[14] The forbidden exciton, Φ_g, also gains strength from the phonon satellite of the allowed state, Φ_u, at slightly higher energy. The joint response of three closely spaced transitions generates the complex electroabsorption spectrum on top of Figure 2 with three positive and two negative peaks within a range of 7 meV. The negative peaks reflect the loss of strength of the allowed transitions, which is transferred to the forbidden state, Φ_g, and generates the positive peak in the center of the spectrum. Additional positive peaks appear at the low- and high-energy side because of the shift of the allowed transitions in the opposite direction. This line shape is repeated in the vibronic progression of a dominant intramolecular vibration of the PMDA molecule of 78.2 meV energy and weaker vibronic replica related to total symmetric vibrations of anthracene, and all of these modes are observed in Raman spectra.[26] Because Raman spectra show no modes below 6 meV, the strongly coupled mode of 3.6 meV seems to be unique to the excited state.[27] The extreme sensitivity of the CT exciton results from the loss of the inversion symmetry of the crystal in an electric field, which is further confirmed by reflectance spectra of isotopically mixed crystals with fluctuations of the lattice potential.[28]

The CT exciton and all vibrational satellites couple only to light with polarization $\vec{e}\|c$. Integration of the spectrum of the imaginary part of the dielectric constant delivers the oscillator strength, f, and the transition dipole, μ_0. Their spectral distribution (Figure 3) shows that the CT exciton is well separated from other excitations. A weak absorption peak at 3.06 eV and stronger and broader peaks at 3.53 and 4.15 eV have been assigned to additional charge-transfer excitons.[16] These transitions do not obey an optical selection rule and are close to intramolecular transition energies of anthracene and PMDA. Because none of the molecular symmetry axes coincide with a crystal axis intramolecular, transitions should not show an optical selection rule. The first exciton in anthracene crystals at 3.11 eV is polarized parallel to the short molecular axis, M,[29] which is tilted out of the (010) plane. Oscillator strength and transition dipole of the intrinsic exciton and its vibrational bands are listed in Table 2 together with solution data of anthracene. The 0−1 band belongs to a single vibrational mode of PMDA, whereas the larger strength of the 0−2 band results from additional contributions by several modes of anthracene. The ZPL of the exciton at 2.2715 eV is very weak and contributes only 1% to the 0−0 band. This band accounts for about 40% of the total oscillator strength of the CT exciton up to 2.7 eV, where the last vibronic exciton is resolved. It should be noted that the total transition dipole, μ_0, of the CT transitions is as large as that of the first singlet of the anthracene molecule but much smaller than the charge-transfer dipole, μ_{CT} = 2.3 eÅ.

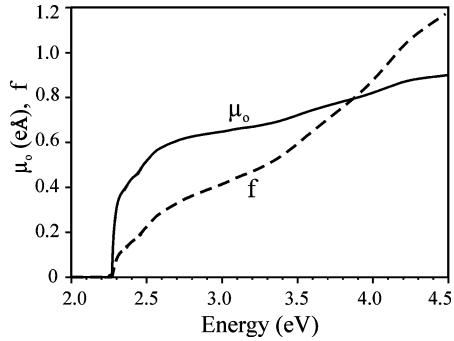

Figure 3. Distribution of oscillator strength, f, and optical transition dipole, μ_0.

TABLE 2: Transition Energy, E, Oscillator Strength, f, and Transition Dipole, μ_0, of the CT Exciton and Its Strongest Vibrational Bands in Comparison with the First Singlet of Anthracene[29]

	ZPL	0−0	0−1	0−2	all	anthracene
E (eV)	2.2715	2.2715	2.350	2.4285	<2.7eV	3.225
f	0.0015	0.126	0.0509	0.0696	0.33	0.305
μ_o (eÅ)	0.05	0.377	0.071	0.075	0.61	0.61

3.2. Extrinsic Transitions. ***3.2.1. Survey of the Spectra.*** Absorption spectra of a 0.35 mm thin crystal in Figure 4 show

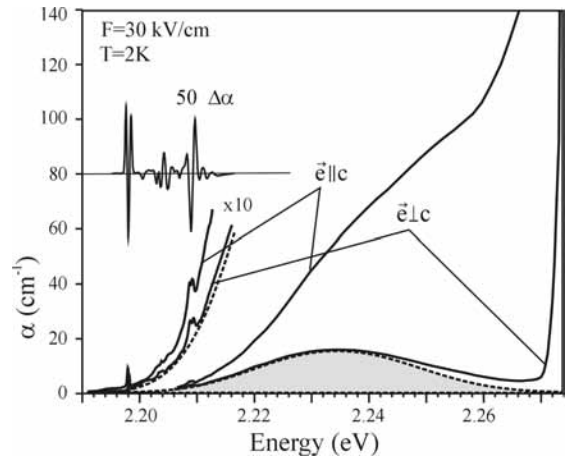

Figure 4. Extrinsic absorption and electroabsorption spectra. The shaded area is a Gaussian fit of the broad absorption band. Part of the spectra are enlarged, as indicated.

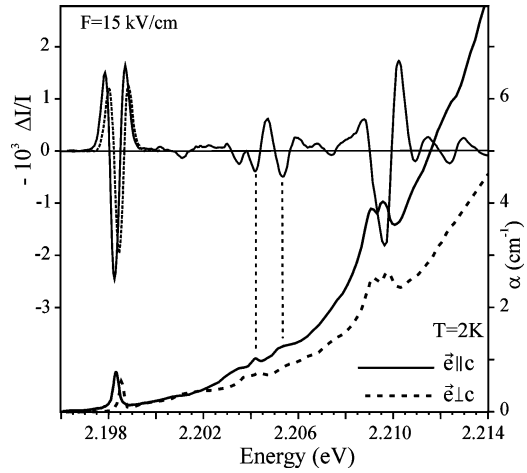

Figure 5. Dependence on the polarization of light of the absorption and electroabsorption spectra in the region of the zero-phonon lines. Sample thickness $d = 2$ mm.

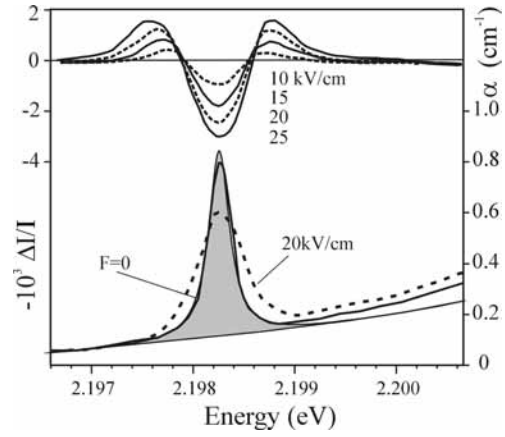

Figure 6. Absorption spectra at zero field and at 20 kV/cm. The shaded area is a Lorentzian fit. The upper part shows electroabsorption spectra at different fields. Sample thickness $d = 1.2$ mm.

a broad absorption band centered at 2.234 eV with three very narrow lines, a singlet and a doublet, on its low-energy tail. They are zero-phonon lines of three transitions with overlapping phonon side bands that match two Gaussian splits by 11 meV. This subgap absorption is nearly isotropic with the spectrum for polarization $e^{\rightarrow}||c$ sitting on the absorption tail of the intrinsic exciton. Because the field $F \perp c$ gave no EA signal in this or any other crystal, the inset shows the EA spectrum of a 1.2 mm thick sample taken with $F||c$. The field 30 kV/cm from the ratio of peak voltage and electrode gap applies to the surface region but decreases deeper in the sample. Scaling the field-induced change of the transmittance to an effective thickness $d = 0.2$ mm results in $\Delta\alpha \approx 0.4$ cm^{-1}, about 50% of the height of the narrow absorption peaks. Assuming a homogeneous field still yields an absorption change that is comparable to the response of the intrinsic exciton. This sensitivity to fields along the molecular stack suggests that the narrow lines belong to charge-transfer excitons that are slightly modified by nearby defects. Integration of the absorption spectrum (eq 5) yields the oscillator strength, f_D, per unit cell. $N = 2.2 \times 10^{21}$ cm^{-3} is the density of unit cells, and the refractive index $n = 1.8$ is estimated from a reflectivity of 8% for $e^{\rightarrow} \perp c$.[16] The defect absorption covers a range similar to that of the 0−0 band of the intrinsic exciton, and assuming the same transition dipole moment, it yields a total defect concentration of 3×10^{-5}. This value exceeds the concentration of impurities in zone-refined materials.

$$f_D = \frac{4m\varepsilon_o c}{e^2 hN} \int_0^\infty n(E)\cdot\alpha(E)\,\mathrm{d}E = 4.40 \times 10^{-6} \qquad (5)$$

Figure 5 presents an expanded view of the extrinsic absorption. The absorption for polarization $e^{\rightarrow}||c$ displays a very narrow line at 2.1983 eV, which is shifted by less than 0.2 meV to higher energy for $e^{\rightarrow} \perp c$, and a similar shift is observed for the doublet near 2.209 eV. This shift probably results from directional dispersion of optical resonances in anisotropic crystals due to a longitudinal field component of the propagating wave.[30] The EA spectrum plotted as relative change of the transmittance of this 2 mm thick crystal does not depend on the polarization of light, as demonstrated by the lowest transition. The small difference in size and energy corresponds to that observed in the absorption spectrum. The negative peak of its EA spectrum coincides with the absorption peak and is framed by two positive peaks of similar height. Further weak signals appear at higher energy, the strongest 6.0 and 7.1 meV above the first transition. They are assigned to vibrational satellites of the first transition because modes of similar energy, 5.8 and 6.8 meV, also appear in the electroreflectance spectrum of the intrinsic exciton.[15]

The EA spectrum of the doublet near 2.209 eV seems different. The strong negative peak coincides with the upper absorption peak, whereas the low-energy peak seems related to a kink in this EA peak. The strong positive peak above the absorption doublet indicates the transfer of oscillator strength to a forbidden state at higher energy, whereas the smaller positive peak at low energy is attributed to some red shift by the Stark effect. It should be noted that the extrinsic excitons do not show the 3.6 meV progression, and satellites pointing to modes of 2.8 and 5.2 meV energy are too weak to affect the line shape of the electronic EA spectrum. No EA signal is found above 2.216 eV in the range of the broad phonon band.

3.2.2. Field-Strength Dependence of the Spectra. Valuable information is gained from the field-strength dependence of the spectra. The shaded area in Figure 6 is a Lorentzian fit of 0.25 meV width to the ZPL line at 2.1983 eV. The absorption peak broadens at 20 kV/cm, and the difference to the zero-field absorption agrees with the shape of the EA spectrum. The EA signal saturates for all samples in a range between 15 and 25 kV/cm, and the spectrum broadens symmetrically with increasing field: the negative peak keeps its position, and positive peaks shift in the opposite direction.

The line shape changes at higher field, as demonstrated in Figure 7 by the sample with the highest defect concentration. The shaded area represents a 0.3 meV wide Lorentzian matched to the transition at 2.1983 and 0.5 meV broad Lorentzians for the doublet at 2.209 eV. Subtracting the phonon sideband indicates that the upper transition is about 20% weaker but still twice as strong as the peak at 2.1983 eV. A field of 35 kV/cm broadens all absorption peaks, and the doublet merges to a flat structure, which vanishes at 50 kV/cm under the phonon sideband.

The larger defect concentration increases the EA signal of the lowest transition at 2.198 eV, but the line shape at 20 kV/cm agrees with that of the previous example in Figure 6. At larger fields, the positive peaks separate from the negative peak, which still keeps its position, and at 50 kV/cm, they appear as distinct peaks of similar height. The slow decrease in the signal amplitude with increasing field is attributed to the inhomogeneity

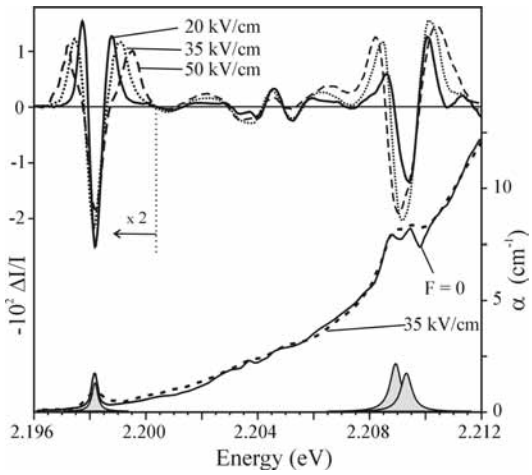

Figure 7. Absorption and electroabsorption spectra of a sample with strong defect absorption. The shaded area represent Lorentzians fits. The EA spectrum below 2.2 eV is enlarged by a factor of two. $T = 2$ K; sample thickness $d = 1$ mm.

of the field. The EA spectrum of the doublet at 2.209 eV behaves differently. The asymmetric line shape at 20 kV/cm becomes more symmetric at higher fields because of the significant increase in the positive peak at low energy. The positive peaks shift in opposite directions, but the negative peak also shifts toward the low-energy absorption peak.

4. Discussion

4.1. Modeling the Extrinsic Spectra. ***4.1.1. Structural Defects.*** Extrinsic and intrinsic excitons respond very sensitively to fields $F\|c$ but not to orthogonal fields. Because the transition energies are similar, the subgap absorption is attributed to donor−acceptor pairs near a defect that must be a structural defect because the purity of the material excludes impurities of sufficient concentration. Furthermore, the defect must not change the orientation of the CT dipole, which excludes charge transfer from regular lattice sites to interstitial molecules between the molecular stacks.

Thermodynamics predicts point defects to be the most abundant lattice defects. Their number, n_j, is given by the minimum of the Helmholtz free energy, U_j-TS_j, where U_j is the energy of formation while the configuration entropy, S_j, increases with the number, N_j, of sites available for such defect.[31]

$$n_j = N_j \exp \frac{-U_j}{kT} \tag{6}$$

The concentration $\eta = n/N$ of vacancies near the melting point reaches, in most metals and weakly bound crystals, 10^{-4}[32] and decreases at lower temperature as long as the activated diffusion enables their migration to external and internal surfaces. The simplicity of the crystal, two sublattices with a single molecule in the unit cell, leaves few options: a vacancy or an antisite defect, a molecule placed into the wrong sublattice. These configurations are sketched in Figure 8 and show that each defect generates a pair of molecular stacks with reversed stacking order.

Such reversal of the stacking order also occurs at stacking faults such as ...ADAD(AA)DADA... However, the misplaced molecule in (AA) displaces all consecutive molecules by $c/2$, and their stack is no longer aligned to neighboring stacks until another stacking fault, (AA) or (DD), restores that alignment.

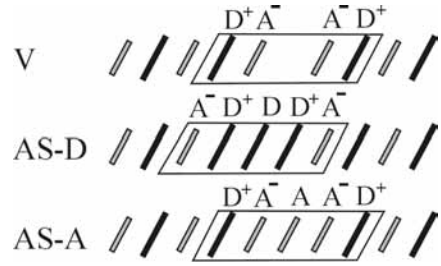

Figure 8. Defects of a donor−acceptor stack with equivalent ionized donor−acceptor pairs in neighbored cells.

(See Figure 1.) A stacking fault therefore leads to a linear defect of energy, U, that increases with the length of the misaligned segment, whereas the number of available sites decreases, which reduces the entropy. All defects in Figure 8 avoid such misaligned stacks and have smaller formation energy and larger configuration entropy because only a single site is modified.

The inversion symmetry of molecules and lattice has an important consequence. Removing or misplacing a molecule creates a local inversion center, whereas molecules in the unit cells next to the defect lose that property and have CT excitons with dipole moments, μ_{CT}, of opposite sign. These excitons are degenerate unless they interact across the defect. The box in Figure 8 with two donor−acceptor pairs separated by the defect thus provides the smallest entity to model extrinsic excitons, $\Psi_{u,g}$, of different parity that comply with the local inversion center. Formally equivalent to the model designed for the intrinsic exciton, intersite hopping splits the pair of excitons next to the defect by 2 V, and coupling their CT dipole to the electric field converts them back to excitons with dipole moments of opposite signs.

To support this formal equivalence, we modeled the EA spectra by the Stark effect with some limitation due to the inhomogeneous field. The relative change of the transmitted intensity is different in thin sheets along the optical path but adds up to the relative change of the transmittance of the sample. Only the field component parallel to the stacking axis contributes to the signal, and because it saturates for fields larger than 15−20 kV and decreases for small fields, the EA spectra are generated in the volume where $F\|c$ exceeds 15−20 kV/cm. Surface fields of 20 kV/cm therefore provide spectra similar to those found with a homogeneous field and an effective crystal thickness on the order of 0.2 mm.

4.1.2. Excitons Next to a Vacancy. The vacancy separates donor−acceptor pairs by a lattice constant resulting in negligible coupling and $V = 0$. Donor and acceptor vacancies cannot be distinguished. CT transitions in unit cells next to the vacancy then produce a single absorption peak. The electric field lifts the degeneracy and the excitons split by the linear Stark effect. Figure 9 presents spectra calculated from the linear Stark effect of a degenerate pair of excitons and matched to the data in Figure 7. The shaded area is the 0.3 meV Lorentzian fit to the absorption peak, whereas the thick line shows the broadened experimental absorption at 20 kV/cm. The calculation assumes a homogeneous field and a dipole moment $\mu_{CT} = 2.2$ eÅ. A field of 20 kV/cm splits the degenerate exciton peak by 0.9 meV into a doublet, which is not resolved in the experiment because much smaller fields in most of the 1 mm thick crystal leave the absorption peak nearly unchanged. Fields of 35 and 50 kV/cm increase the volume with large field which broadens the absorption peak until it disappears in the background absorption in agreement with the experiment.

The calculated EA spectra, $\Delta\alpha$, are the difference of Lorentzian absorption peaks with and without the homogeneous

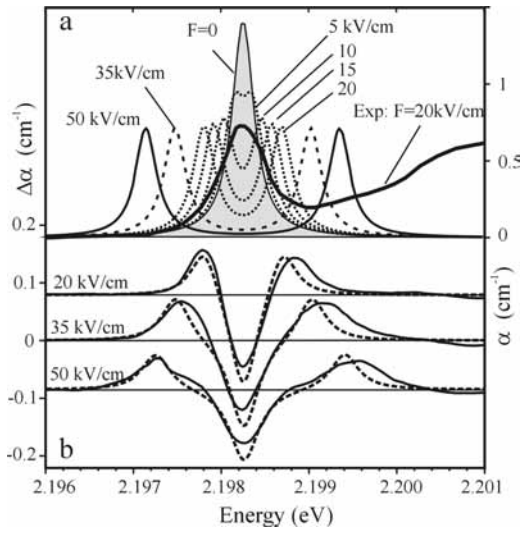

Figure 9. (a) Lorentzian fit to absorption spectrum in Figure 7 and its shape in an electric field. (b) Experimental (full curves) and modeled (dotted) electroabsorption spectra.

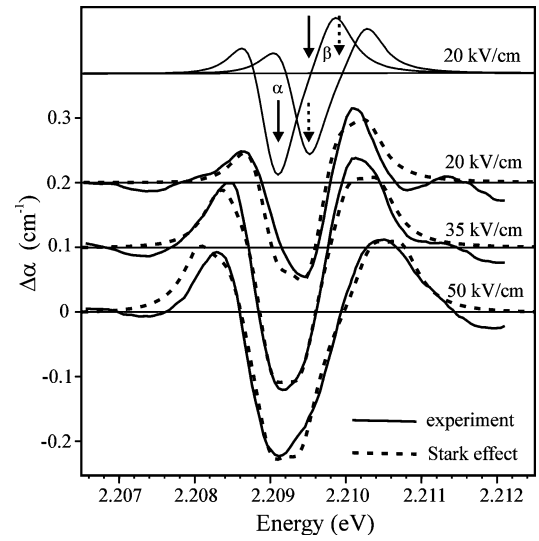

Figure 10. Experimental and modeled EA spectra for different fields. Full and dashed arrows mark the energy of pairs of dipole-allowed and -forbidden excitons, which are mixed by the field. The upper curves show the response of each pair α and β at 20 kV/cm.

field and scaled down by a factor of seven to eight to match the experimental signal height. Because the lock-in amplifier turns out effective values of the Fourier components of ΔI, the peak amplitude of the signal is about twice as large, $\pi/\sqrt{2}$ and $2\sqrt{2}$, for a square-shaped and a harmonic response, respectively. The remaining discrepancy is attributed to the volume with smaller field. The linear Stark shift by $\pm\mu_{CT}F$ of a pair of degenerate excitons reproduces the EA spectra for $\mu_{CT} = 2.2$ eÅ and vanishing zero-field splitting. This agreement confirms also that the inhomogeneous field merely affects the amplitude of the signal. Spectra modeled with a distribution of fields reproduce the EA spectrum too but need a slightly larger dipole moment, 2.4 eÅ, to reproduce the shift of positive peaks.

4.1.3. Excitons Next to Antisite Defects. The other extrinsic purely electronic transition is the doublet near 2.209 eV. If it belongs to excitons on the same defect that get mixed by an electric field, then they would shift in opposite directions. The assumption of a pair of dipole-allowed excitons next to a defect excludes that this defect is an inversion center, which leads to obvious discrepancies of predicted and observed EA spectra. The different height of the positive EA peaks requires faster shift and larger dipole moment of the upper transition. Furthermore, the EA spectrum should have two negative peaks coinciding with the absorption peaks, and the spectral line shape should not change with increasing field. The experiment shows a single negative peak that shifts with increasing field, and the spectral line shape is more symmetric at high field. These inconsistencies disappear if the absorption doublet belongs to different defects, α and β, which are inversion centers. Each absorption peak corresponds to a dipole-allowed exciton, which is coupled by an electric field to a corresponding dark state of even parity. Antisite defects, a donor molecule in the acceptor sublattice, and vice versa provide such defects. The misplaced molecule should improve intersite hopping, resulting in some zero-field splitting, $2V$. The field-induced change, Δα, depends on the ratio $\rho = \mu_{CT}F/V$ and yields for $\rho \ll 1$ a quadratic Stark effect, as observed for the intrinsic exciton at small field.[14,15] This weak perturbation regime breaks down for $\rho \approx 1$, and dark and bright excitons are converted to excitons of similar strength, which split further apart by the Stark shift.

Figure 10 compares electroabsorption spectra near 2.209 eV with calculated spectra based on 0.4 meV broad Lorentzians matched to the absorption peaks. The calculated spectra are scaled down again by a factor of seven and assume a charge-transfer dipole $\mu_{CT} = 1.8$ eÅ. Full and dashed arrows mark for each antisite defect α and β the position of the dipole-allowed and -forbidden excitons, respectively. The transition energy of the allowed excitons differs by 0.4 meV, and this value is also assumed for the zero-field splitting by $2V$ of pairs of different parity. Because the Stark shift by 0.36 meV in a field of 20 kV/cm is already twice as large as V, bright and dark states are converted already transformed to excitons of equal strength. Calculated spectra of each pair α and β for 20 kV/cm are shown at the top of Figure 10. The negative peak coincides with the absorption peak and shows its loss of strength, which is transferred to the formerly forbidden state, Ψ_g. Both transitions shift in opposite directions, which creates a positive peak on either side of the negative peak. The Δα peak at high energy, however, is larger because in addition to the Stark shift, oscillator strength has been moved to a dark state at higher energy. This asymmetry vanishes for $V = 0$ but always appears for finite zero-field splitting. The sum of the EA spectra of α and β reproduces the experimental spectrum at 20 kV/cm quite satisfactorily. The negative peak of the spectrum of α is partially compensated by the positive peak due to the red shift of the lower state of the pair β. Such compensation occurs not for the negative peak of β because the blue shift of the forbidden exciton α moves oscillator strength already beyond that transition. The negative peak of the EA spectrum thus coincides with the upper peak of the absorption doublet.

The line shape of the EA spectrum strongly depends on the splitting of the absorption peaks, their spectral width, and the zero-field splitting of dark and bright excitons relative to the Stark term $\mu_{CT}F$. If the field term exceeds the other energies, then the same oscillator strength is transferred into a range of negligible zero-field absorption above and below the absorption doublet resulting in symmetric positive Δα peaks. This increasing coupling strength to the field explains why the EA spectrum changes with increasing field from an asymmetric to a more symmetric line shape. Because at larger field the loss of strength of the low-energy exciton, α, is no longer compensated by the Stark shift of the upper exciton, β, both allowed excitons contribute to a broad negative peak of the EA spectrum, which shifts its center to lower energy. This gradual change of line

TABLE 3: Transition Energy, E_0, Zero-Field Splitting, V, and the CT Dipole, μ_{CT}, of the Intrinsic CT Exciton (CT) and Excitons Next to a Vacancy or an Antisite Defect

transition	CT	V	AS-α	AS-β
E_0 (eV)	2.2713	2.19826	2.2092	2.2096
V (meV)	0.8	0	0.2	0.2
μ_{CT} (eÅ)	2.3	2.2 to 2.4	1.8	1.8

TABLE 4: Character Table of the Irreducible Representations of Crystal States

	$\{E\}$	$\{I\}$
Γ_1	1	1
Γ_2	1	–1

shape is reproduced by a single set of parameters, and matching the signal height confirms that the lower transition is about 20% stronger. A consistent fit of the EA spectrum at low field is possible only if the dark state of α has about the same transition energy as the bright state of β. Increasing the splitting of the absorption peak to 0.5 meV or reducing 2 V to 0.3 meV leads to poorer agreement of calculated and experimental spectra. Similarly, small variation is possible for the spectral line width. The fit improves by assuming a slightly smaller CT dipole moment, 1.6 eÅ, for the lower transition, but in view of the uncertainty arising from the inhomogeneous field, no attempt is made to refine the model further.

4.2. Properties of Charge-Transfer Excitons. The sensitivity of extrinsic and intrinsic excitons to an electric field results from near-degeneracy of states of different parity and the large charge-transfer dipole, μ_{CT}, in a unit cell. Table 3 lists the transition energies, E_0, zero-field coupling, V, and CT dipole of the intrinsic exciton CT and extrinsic excitons in unit cells next to a vacancy, V, or an antisite, AS. The similar properties prove that the donor−acceptor pair of a unit cell is the fundamental part of all CT excitons, whereas the small zero-field splitting confirms weak coupling by intersite hopping over the distance of a lattice constant. The smaller transition energies of extrinsic excitons point to minor rearrangement of donor−acceptor pairs by a nearby defect. Because the global inversion symmetry is lost, dimerization could occur, which likely increases the ground-state energy and increases the Coulomb coupling in the excited state. However, the decrease in energy by 60−70 meV is sufficient for suppressing mixing of extrinsic and intrinsic excitons by electric fields.

Extrinsic excitons are attributed to unit cells next to a local inversion center, a vacancy, or a misplaced molecule. Excitons next to a vacancy remain degenerate, and their vanishing zero-field splitting is consistent with localization of excitons to a molecular stack. They therefore represent the excited state of a unit cell and have the same charge-transfer dipole moment as the intrinsic exciton, which represents the CT dipole moment per unit cell. Improved coupling across a misplaced molecule leads to a small zero-field splitting of dark and bright excitons attributed to the unit cell next to an antisite defect. This defect is a string of three donor or acceptor molecules, but such equivalence of three molecular states is lost in the excited state, and excitons again are linear combinations of donor−acceptor pairs on either side of the misplaced molecule. Residual coupling of electron or hole to the equivalent state of the antisite molecule may explain the smaller CT dipole moment of excitons next to antisites and their splitting into an absorption doublet.

The lack of an optical selection rule of extrinsic excitons is the main difference from intrinsic excitons, which is particularly striking in view of the common selection rule $F \| c$ of the Stark effect. Optical transitions and the Stark effect involve dipole matrix elements that must comply with the symmetry of the states. An ionized pair $A^-D^+ = \Phi_2$ has a permanent dipole moment, μ_p, which is the expectation value $\langle e\vec{r} \rangle$ in this state.

$$\vec{\mu}_p(2) = e\langle \Phi_2 | \vec{r} | \Phi_2 \rangle \tag{7}$$

Because anthracene and PMDA have inversion symmetry, the charge distribution is centered on the molecular sites and the permanent dipole points along the connecting line resulting in $\mu_p \| c$. In case of a neutral ground state, Φ_1, the permanent dipole, $\mu_p(2)$, is identical to the CT dipole, μ_{CT}, which determines the Stark effect of the exciton. The model can be extended to hybridized molecular HOMO and LUMO states, which adds an ionic contribution to the ground state and a neutral contribution to the excited state. The centers of charge in the ground and in the excited state still fall on the c axis but are displaced from the molecular sites. The optical transition corresponds to partial charge transfer over the intermolecular distance, and μ_{CT} of the exciton is the difference, $\Delta\mu_p$, of the permanent dipoles in the excited state, Φ_2, and in the ground state, Φ_1.

Permanent dipoles appear in systems with inversion symmetry only if states of different parity, Φ_u and Φ_g, are degenerate and have a nonvanishing transition dipole matrix element.

$$\vec{\mu}_p(g,u) = e\langle \Phi_u | \vec{r} | \Phi_g \rangle \tag{8}$$

Because both excited states are linear combinations of ionized donor−acceptor pairs, the field-induced dipole is again the permanent dipole, μ_p, of an ionized pair. The absence of any measurable response to $F \perp c$ confirms the negligible coupling of molecules in different stacks, which would provide dipoles with components perpendicular to the molecular stack.

The optical transition dipole, μ_0, represents an electron that oscillates with the frequency of light between the ground and the excited state.

$$\vec{\mu}_0 = e\langle \Phi_2 | \vec{r} | \Phi_1 \rangle \tag{9}$$

Because the oscillator strength scales with the probability of finding the electron at the position of the hole,[33] only excitons with partial charge transfer absorb light. The stacking of donor and acceptor molecules leads to a component of μ_0 parallel to c, but orthogonal components also occur if the spatial distribution of the electron c is different in the ground and the excited states. With the molecular planes tilted out of the ac plane, intramolecular transition dipoles couple to light according to their projection onto the polarization of light. The different shape and size of the HOMO of anthracene and the LUMO of PMDA make it unlikely that the charge-transfer exciton does not couple to light-polarized perpendicular c. The absence of an optical selection rule of the extrinsic CT excitons is thus in accordance with the low symmetry of the crystal and suggests that the optical selection rule of the intrinsic exciton that arises is related to the translation invariance of crystal states, a symmetry that does not apply to excitons near defects.

4.3. Role of Translation Invariance. Near-degenerate states of different parity are needed to explain the Stark effect of the intrinsic charge-transfer exciton. The current model is based on trimer configurations, which by intersite hopping change the orientation of their dipole moment from AD^+A^- to A^-D^+A and

provide by linear combination dark and bright excitons split by 1.6 meV. However, because this intersite hopping occurs between translational equivalent sites, it broadens the LUMO and HOMO states into conduction and valence bands rather than splitting the single CT exciton of a unit cell into a pair of states. The width of the resulting exciton band is not known, but from doubling of a vibronic satellite in isotopically mixed An−PMDA crystals, a value of 12 meV has been estimated.[28] Larger electronic bandwidth of 200 meV has been estimated from the close contact of molecules within the donor−acceptor stack, which for the exciton may be reduced by polaronic coupling.[12]

The current model ignores the fact that a single donor−acceptor pair in a unit cell provides only a single CT exciton and neglects the fact that inversion symmetry is linked to the translation symmetry of the lattice. Because optical selection rules are related to symmetry, we take a look at the prediction of group theory for crystal states.[2] The identity $\{E\}$ and inversion $\{I\}$ as only point symmetries lead to two irreducible representations of crystal states and a simple character table.

The valence band state, derived from even parity HOMO states, is represented by Γ_1, whereas the odd parity LUMO states generate a conduction band state of Γ_2 symmetry. The internal motion of the excited electron hole pair bound by the Coulomb potential is described by an envelope function, ψ, which has either Γ_1 or Γ_2 symmetry, and the direct product of these states, representing hole, electron, and the internal motion, defines the symmetry Γ_X of the exciton.

$$\Gamma_X = \Gamma_\psi \otimes \Gamma_2 \otimes \Gamma_1 \tag{10}$$

Because only excitons of type Γ_2 are dipole-allowed, the envelope ψ must have even parity in the case of a dipole-allowed interband transition, Γ_1 to Γ_2. The lower-lying bright exciton is thus the symmetric linear combination of donor−acceptor pairs, $A^+D^- + D^-A^+$, whereas the antisymmetric envelope function leads to a forbidden exciton state at higher energy. This assignment reverses that of the trimer model, which neglected the symmetry of the molecular ground and excited state and their coupling to valence and conduction bands. Indeed, bright excitons in semiconductors with dipole-allowed interband transitions have s-type envelope functions, whereas p-type excitons appear if the interband transition is forbidden. These p-type excitons have very low oscillator strength because the envelope function vanishes at the position of the hole.[33] A symmetric envelope function is consistent with the strength of the intrinsic CT exciton, and the forbidden state may be an excited exciton state with a p-type envelope. Although that provides a simple explanation for a pair of excitons of different parity, the zero-field splitting by 1.6 meV seems far too small in view of the strong Coulomb potential at intermolecular distance.

We therefore take a closer look at the band states in eq 10, which are part of the exciton. Translation invariance leads to Bloch states $\Phi_j = \exp(ikr)u_{j,k}(r)$, where the plane wave envelope describes the free motion of a particle in an energy band, $E_j(k)$, and modulates the lattice periodic state, $u_{j,k}(r)$, in the unit cells. An−PMDA consists of two lattices with a centrosymmetric molecule on the lattice points. Intermolecular coupling is weak because of the large lattice constants, and the lattice periodic part, $u_{j,k}(r)$, differs little from the molecular eigenstates. The sublattices are displaced by half a lattice constant and exchange charge under illumination. The resulting CT exciton is modeled as linear combinations of Bloch states of both sublattices, and for the sake of simplicity, we neglect hybridization. With the anthracene sublattice as reference, the displacement of the PMDA sublattice by $+c/2$ or $-c/2$ introduces a phase factor $\exp(\pm ikc/2)$ to the conduction band states. Either displacement generates the same periodic potential, and linear combinations of these phase factors provide even and odd parity conduction band states from the LUMO state, Φ_A, of the acceptor.

$$\Phi_A^{\pm}(k) = \exp(ikr)\frac{1}{\sqrt{2}}[\exp(ikc/2) \pm \exp(-ikc/2)]u_{A,k}(r) \tag{11}$$

$$\Phi_g(k) = \exp(ikr)u_{A,k}(r)\cos\frac{kc}{2},$$

$$\Phi_u(k) = \exp(ikr)u_{A,k}(r)\sin\frac{kc}{2}$$

These states are degenerate because the phase difference $\pi/2$ of cos $kc/2$ and sin $kc/2$ has no effect on the spatial distribution of an electron in the LUMO state, which is recovered by Fourier transformation of the conduction band. The electric field removes this degeneracy by the energy, which, depending on the direction of the charge transfer, is gained or lost. The linear Stark effect of an intrinsic exciton with a symmetric envelope function then arises from equivalent ways to generate the crystal by the addition of the acceptor sublattice to the lattice set up by the donor.

The small zero-field splitting of the exciton with a symmetric envelope function then must result from interactions that have not yet been considered. One obvious interaction is the coupling of the transition dipole to eigenmodes of electromagnetic waves, which splits the dipole-allowed exciton states, $E_X(k)$, and the electromagnetic mode, $\gamma(k)$, into two branches of a polariton, $\Omega(k)$.[34] The splitting is on the same order as the gap between transverse and longitudinal excitons, which increases with the oscillator strength of the exciton and the density of states.[30] The strength of the ZPL yields a gap of 0.4 meV, which increases to 3 meV if the oscillator strength of the 0−0 band is taken. Polariton coupling decreases the energy of the dipole-allowed exciton, whereas the forbidden exciton without coupling to radiation modes needs no renormalization. Coherent coupling of the intrinsic exciton, $E_X(K)$, to elastic modes of the lattice generates the progression of 3.6 meV in the spectra of the intrinsic exciton. This mode must have Γ_1 symmetry to maintain the symmetry of the dipole-allowed exciton. Extrinsic excitons, in contrast, do not form polariton states or coherently coupled states with phonons because the defect scatters propagating waves.

Translation symmetry also explains the optical selection rule of intrinsic excitons. Optical transitions between band states are described by the momentum matrix element and obey the k-selection rule, $\Delta k \approx 0$, because of the long wavelength of light. The large interstack distance and much smaller molecular separation within a stack suggest delocalization along the c axis only, and in this 1D lattice, inversion and mirror symmetry are equivalent. The interband matrix element reflects the charge transfer from the donor to the acceptor sublattice along the c axis and explains the optical selection rule of intrinsic excitons by delocalization along the molecular stack only. Although the Coulomb field of an ionized donor localizes the electron to neighboring acceptor sites, the exciton is delocalized because equivalent donor sites exist in each unit cell, and the corresponding exciton band, $E_X(K)$, describes the center-of-mass motion of an electron−hole pair. Irrespective of the width of

the exciton band, the exciton absorption is a narrow line because the wavevector, K, of this motion must satisfy the k-selection rule.

5. Conclusions

High-quality single crystals of anthracene−pyromellitic dianhydride show narrow exciton lines 60−70 meV below the absorption edge with a much stronger phonon sideband. They respond to an electric field as sensitive as an intrinsic charge-transfer exciton and are attributed to excitons in unit cells next to point defects of a few 10^{-5} concentration. These purely electronic transitions in a simple lattice offer the unique possibility of analyzing the EA spectra by basic quantum mechanics and identify key conditions for the large sensitivity of all excitons to an electric field: narrow spectral width, inversion symmetry, a large dipole moment, and near-degeneracy of excitons of different parity. Excitons of different parity are derived from ionized donor−acceptor pairs, D^+A^-, with a large dipole moment, μ_p, which interact weakly across a point defect with inversion symmetry. The field breaks the inversion symmetry and converts dark and bright excitons into excitons of equal strength when the Stark shift becomes comparable to their splitting.

The unique sensitivity of all excitons to an electric field parallel to the molecular stack rests on a unit cell with two centrosymmetric molecules displaced by half of a lattice constant, which makes each molecular site an inversion center of the crystal. Defects such as vacancies and misplaced molecules provide local inversion centers, and excitons in neighboring unit cells combine to a pair of dark and bright excitons, which split by intersite hopping. Excitons separated by a vacancy remain degenerate, whereas the increased hopping rate across a misplaced molecule splits the excitons by about 0.4 meV. Such small zero-field splitting of localized excitons reveals weak intersite hopping over a lattice constant and confirms negligible coupling of molecules in different stacks.

The CT dipole of excitons next to a vacancy has the same value, 2.2 to 2.4 eÅ, as the intrinsic exciton. Excitons next to misplaced molecules have a slightly smaller CT dipole, 1.8 eÅ, which is attributed to residual coupling of the electron (hole) to the misplaced acceptor (donor) molecule. The similar properties of extrinsic and intrinsic excitons reveals the donor−acceptor pair of a unit cell as the basic unit of all excitons. This explains the orientation of the CT dipole along the molecular stack and imposes no optical selection rule, which is in agreement with the almost-isotropic spectra of extrinsic excitons.

Intrinsic excitons, in contrast, couple only to light polarized along the molecular stack. Their optical selection rule is attributed to delocalization along the stacking axis and negligible interstack coupling, which results in 1D Bloch states. Equivalent relative displacements of donor and acceptor sublattices by half of a lattice constant up or down the molecular stack allows us to model degenerate intrinsic excitons of different parity. That equivalence is lost if electrons gain or lose energy by charge transfer, and the degenerate intrinsic excitons split by a linear Stark effect into a pair of dipole-allowed states of equal strength.

The dark state, 1.6 meV above the intrinsic exciton, could be attributed to an excited exciton state with an asymmetric envelope function. The splitting of an s- and p-type exciton envelope seems to be too small in view of the strong Coulomb field. It may instead result from coupling the exciton to crystal states that are not included in the electronic Hamiltonian. An obvious mechanism is coupling excitons to the radiation modes of the crystal, which converts dipole-allowed exciton into a polariton resonance at lower energy. Coherent coupling to elastic lattice modes is invoked to explain the pronounced progression of the 3.6 meV energy of the intrinsic exciton, which is not observed in the spectra of extrinsic excitons. These differences of extrinsic and intrinsic excitons reveal that translation invariance must not be ignored if the properties of intrinsic excitons are analyzed, even if intermolecular coupling is weak.

Acknowledgment. We thank Norbert Karl, University of Stuttgart, for providing the crystals and pointing out many details of the material. We acknowledge discussions with Stefan Koch, University of Marburg, on delocalized excitons and Zoltan Soos, University of Princeton and Anna Painelli, University of Parma, for discussion of the local aspects of CT excitons.

References and Notes

(1) Davydov, A. S. *Theory of Molecular Excitons*; Plenum Press: New York, 1971.
(2) Yu, P. Y.; Cardona, M. *Fundamentals of Semiconductors*; Springer: Heidelberg, Germany, 1996.
(3) Mullikan, R. S. *J. Am. Chem. Soc.* **1952**, *74*, 811.
(4) Keller, H. J. *Chemistry and Physics of One-Dimensional Metals*; Plenum Press: New York, 1977.
(5) Abbi, S. C.; Hanson, D. M. *J. Chem. Phys.* **1974**, *60*, 319.
(6) Sebastian, L.; Weiser, G.; Peter, G.; Bässler, H. *Chem. Phys.* **1983**, *75*, 103.
(7) Weiser, G. *Phys. Status Solidi A* **1973**, *18*, 347.
(8) Haarer, D.; Karl, N. *Chem. Phys. Lett.* **1973**, *21*, 49.
(9) Haarer, D. *Chem. Phys. Lett.* **1974**, *27*, 91.
(10) Haarer, D. *J. Chem. Phys.* **1977**, *67*, 4076.
(11) Brillante, A.; Philpott, M. R. *J. Chem. Phys.* **1980**, *72*, 4019.
(12) Haarer, D.; Philpott, M. R. In *Spectroscopy and Excitation Dynamics of Condensed Molecular Systems*; Agranovich, V. M., Hochstrasser, R. M., Eds.; North Holland Pub. Co.: New York, 1983.
(13) Haarer, D. *Chem. Phys. Lett.* **1975**, *31*, 192.
(14) Haarer, D.; Philpott, M. R.; Morawitz, H. *J. Chem. Phys.* **1975**, *63*, 5238.
(15) Elschner, A.; Weiser, G. *Chem. Phys.* **1985**, *98*, 465.
(16) Merski, J.; Eckhardt, C. J. *J. Chem. Phys.* **1981**, *76*, 3705.
(17) Weiser, G. *J. Lumin.* **2004**, *110*, 189.
(18) Port, H.; Hartschuh, A. *J. Lumin.* **2004**, *110*, 315.
(19) Mazumdar, S.; Guoa, F.; Meissner, K.; Fluegel, B.; Peyghambarian, N.; Kuwata-Gonokami, M.; Sato, Y.; Ema, K.; Shimano, R.; Tokihiro, T.; Ezaki, H.; Hanamura, E. *J. Chem. Phys.* **1996**, *104*, 9283.
(20) Karlin, N. *Crystal Growth, Properties, and Applications*; Freyhardt, H. C., Ed.; Springer: Berlin, 1980.
(21) Boeyens, J. C. A.; Herbstein, F. H. *J. Phys. Chem.* **1965**, *69*, 2153.
(22) Robertson, B. E.; Stezowski, J. J. *Acta Crystallogr.* **1978**, *B34*, 3005.
(23) Massa, D.; Karl, N. *Mol. Cryst. Liq. Cryst.* **1989**, *95*, 93.
(24) Boeyens, J. C. A.; Herbstein, F. H. *J. Phys. Chem.* **1965**, *69*, 2160.
(25) Mrozek, J.; Petelenz, P.; Smith, V. H., Jr. *Chem. Phys. Lett.* **1982**, *85*, 245.
(26) Syme, R. W.; Morawitz, H.; Macfarlane, R. M. *Solid State Commun.* **1979**, *32*, 1059.
(27) Petelenz, P.; Siebrand, W. *Chem. Phys. Lett.* **1982**, *82*, 427.
(28) Tokura, Y.; Koda, T. *Solid State Commun.* **1981**, *40*, 299.
(29) Philpott, M. R. *J. Chem. Phys.* **1969**, *50*, 5117.
(30) Weiser, G. In *Photophysics of Molecular Materials*; Lanzani, G., Ed.; Wiley-VHC: Weinheim, Germany, 2006.
(31) Henderson, B. *Defects in Crystalline Solids*; Edward Arnold: London, 1972.
(32) Franklin, A. D. In *Point Defects in Solids*; Crawford, J. H., Slifkin, L. M., Eds.; Plenum Press: New York, 1972; Vol. 1.
(33) Elliott, R. J. *Phys. Rev.* **1957**, *108*, 1384.
(34) Hopfield, J. J. *Phys. Rev.* **1958**, *112*, 1555.
(35) Karl, N. In *Landolt Börnstein Tables, New Series*; Madelung, O., Schulz, M., Weiss, H., Eds.; Springer: Heidelberg, 1985; Vol. 17i.

JP901300K